

Supporting information for:

Reactive Oxygen Species Activated AIEgen for bacterial membrane destruction and antibacterial photodynamic therapy of Methicillin-Resistant *Staphylococcus aureus*

Lin Kong, Rongyuan Zhang, Junyi Gong, Huan Wang, Lingyu Zhai, Dongfeng Dang, Qian Liu, Zheng Zhao, Ben Zhong Tang

Contents

S1 Experimental section

S2 Optical properties of MNNPyBB

S3 Bacterial toxicity of MNNPyBB with or without light

S4 Toxicity of MNNPyBB in treated mice

S5 Optical properties and bacterial toxicity of intermediate MNNPy

S1 Experimental section

ROS Detection

The ROS levels were quantified using 2,7-dichlorodi-hydrofluorescein diacetate (DCFH-DA), which was turned to 2,7-dichlorofluorescein (DCF, emits green fluorescence, λ_{ex} : 488 nm, λ_{em} : 525 nm) represented ROS release. The fluorescence intensity of DCF was measured after addition with MNNPyBB or Ce6 over a period of light exposure from 0 to 120 second.

For singlet oxygen detection, the electron paramagnetic resonance (EPR) assay was conducted at room temperature using a Bruker Nano x-band spectrometer. 5,5-dimethyl-1-pyrroline N-oxide (DMPO) served as the spin-trap agent. MNNPyBB was dissolved in methanol at a concentration of 1.0 mmol L⁻¹, and subsequently 25 mmol L⁻¹ DMPO was added into methanol without or with light irradiation (wLED, 100 mW cm⁻²) for 30 s.

Bacteria Culturing, Staining, and Imaging

All bacterial strains used in this study were listed in [Table S1](#). After culturing in LB broth medium at 37 °C with a shaking speed of 180 rpm for 12 h, *E. coli*, *B. proteus*, *S. aureus*, *B. cereus*, *B. subtilis* and MRSA were harvested by centrifuging at 5000 rpm for 5 min at 4°C and subsequently washed twice with phosphate buffered saline (PBS, pH 7.4). Then, 1 μ L of MNNPyBB (1 mmol L⁻¹) was added to the bacteria suspension (1×10^9 CFU mL⁻¹) and incubated at 37 °C with a shaking speed of 180 rpm for 10 min. To take fluorescence images, 0.5 μ L of MNNPyBB-stained bacteria suspension was transferred onto a glass slide and covered with a coverslip. The images were captured using a confocal microscopy (Leica SP8, Germany).

Bacterial Morphological Characterization

Bacterial cultures of MRSA were grown in LB broth medium and then resuspended into *dd*H₂O to achieve a cell density of $\approx 10^{10}$ CFU mL⁻¹. The cultures were treated with MNNPyBB (10 μ mol L⁻¹) without or with white light irradiation for 30 min. Following the treatment, the bacteria were collected, washed with *dd*H₂O and resuspended in *dd*H₂O for analysis by field emission scanning electron microscopy (FE-SEM, S4800) after gradient dehydration by ethanol of different concentrations. For transmission electron microscopy (TEM, HT7700) analysis, the MNNPyBB-treated bacteria was incubated at 37 °C with a shaking speed of 180 rpm for 30 min followed by exposure to white light for an additional 30 min. The bacteria were then harvested by centrifugation at 5000 rpm for 5 min and fixed with 2.5% glutaraldehyde. Control samples included bacteria without any treatment and those incubated with MNNPyBB alone.

Theoretical calculation

The membrane penetration process was simulated by GROMACS 2022.1 accelerated by CUDA 11.7 with bilayer systems topology constructed by Packmol. The bilayer system was simulated under the Slipid 2020 force field, which was

compatible with the general amber force field (GAFF) [S1-S6]. The GAFF was applied on the small molecule with self-optimized parameters of boron-containing bonds. The original molecule structure of MNNPyBB was optimized by ORCA 5.0.2 under BLYP-D4/def2-SVP level and used to calculate the single point energy under B3LYP/def2-TZVP level [S7-S8]. The RESP model, which was implemented by multiwfn package, was utilized to calculate the atomic charge [S9-S10].

Antibacterial evaluation *in vitro*

To evaluate the antibacterial efficacy of MNNPyBB in combination with white light exposure, MRSA cultures were first incubated overnight and then diluted to 1×10^9 CFU mL⁻¹. Subsequently, 95 μ L of MRSA suspension were added into a 1.5 mL eppendorf (EP) tube containing 5 μ L of MNNPyBB achieving a final concentration of 10-50 μ mol L⁻¹. The mixture was incubated at 37 °C for 30 min, followed by exposure to white LED for durations ranging from 5-30 min, with some samples not receiving light exposure. After this, bacterial suspension was diluted with liquid LB medium at a 1:10⁴ ratio. 100 μ L of the dilution was then plated on LB agar plates. Post-overnight incubation at 37 °C, the number of bacterial clone was counted for calculating relative bacterial colony counts. The experiments were conducted in triplicate.

Mouse bacterial infection and inflammation model

Animal experiments were conducted in strict compliance with the guidelines of the Research Ethics Committee of AnHui University (approved protocol number: IACUC(AHU)-2022-051). 6-8 weeks old Balb/c mice with 20 g average weight were acquired and housed under specified pathogen-free environment for 3 days. Four groups of mice (n = 5) were intraperitoneally infected with 20 μ L of bacterial suspension (2×10^8 CFU per mouse) and their survival was monitored daily. After 24 h post-infection, mice in group IV underwent a 30 min treatment with MNNPyBB (20 μ L of 1 mmol L⁻¹), followed by another 30 min of white light exposure (150 mW cm⁻²). In contrast, group I received a PBS treatment as a blank control, group II was subjected to 30 minutes of white light irradiation (150 mW cm⁻²) as a light control, and group III received MNNPyBB (20 μ L of 1 mmol L⁻¹) as a MNNPyBB control. The healing progress was tracked daily through photographs of the wounds. The wound area was subsequently measured and analyzed using ImageJ software. The wound closure percentage (%) was calculated by comparing the healed wound area to the initial. The healed area was determined as the difference between the initial and current wound area. Additionally, the mice weight was recorded daily after treatment.

For the assessment of bacterial burden, mice were sacrificed after experiments. The heart, liver, spleen, lungs, kidneys, and a section of the infected skin tissue were collected and homogenized in a 4% paraformaldehyde solution for subsequent pathological sectioning, and then hematoxylin-Eosin (H&E) staining. Histological images were captured using an inverted microscope (Olympus, IX71, Japan). Histopathological changes were alterations were evaluated based on a standard H&E staining protocol. The experiments were carried out in Wuhan servicebio technology

CO., LTD.

Another segment of the infected skin was reserved for ELISA assays. The survival of MRSA in the wounds after different treatments was also evaluated as well. The skin and subcutaneous tissues surrounding the wounds were excised and homogenized in PBS. The homogenates were subsequently plated onto LB agar plates for the quantification of bacterial colonies. Blood samples from the four experimental groups were also diluted and analyzed.

Cytotoxicity assays (MTT method)

The cytotoxicity of MNNPyBB on living NIH3T3 and BEND.3 cells was measured using a 5-dimethylthiazol-2-yl-2,5-diphenyltetrazolium bromide (MTT) assay.

Cytokines level

The testing of cytokines in colonic protein extracts was carried out in Shanghai Jianglai Industrial Limited by Share LTD, using relevant ELISA kits and strictly following the manufacturer's instructions. Protein extracts were isolated by homogenization of skin segments. Samples were centrifuged at 30000 g for 20 min and stored at -80 °C until cytokine determination.

Statistical analysis

Data were shown as mean \pm SD (standard deviation). Differences between groups were assessed using the Student's T-test. $P < 0.05$ was considered as statistically significant ($\#p > 0.05$, $*p < 0.05$, $**p < 0.01$ and $***p < 0.001$).

S2 Optical properties of MNNPyBB

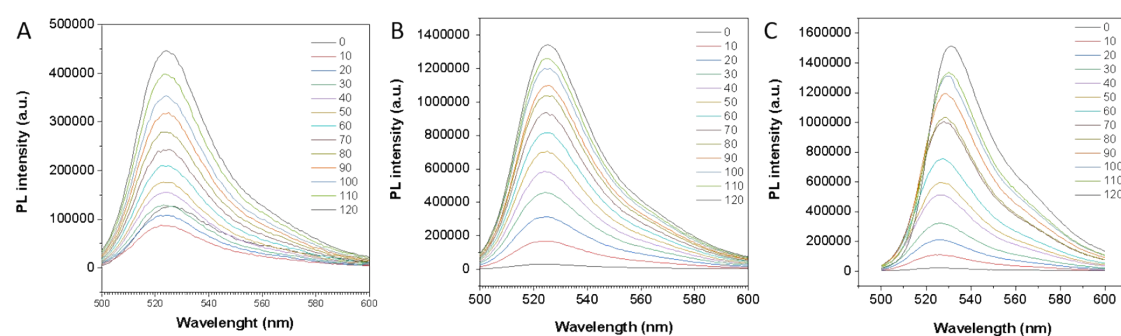


Figure S1 (A) Fluorescence emission of DCF-DA under light irradiation in NaOH solution, and with the assistance of (B) Ce6 and (C) MNNPyBB.

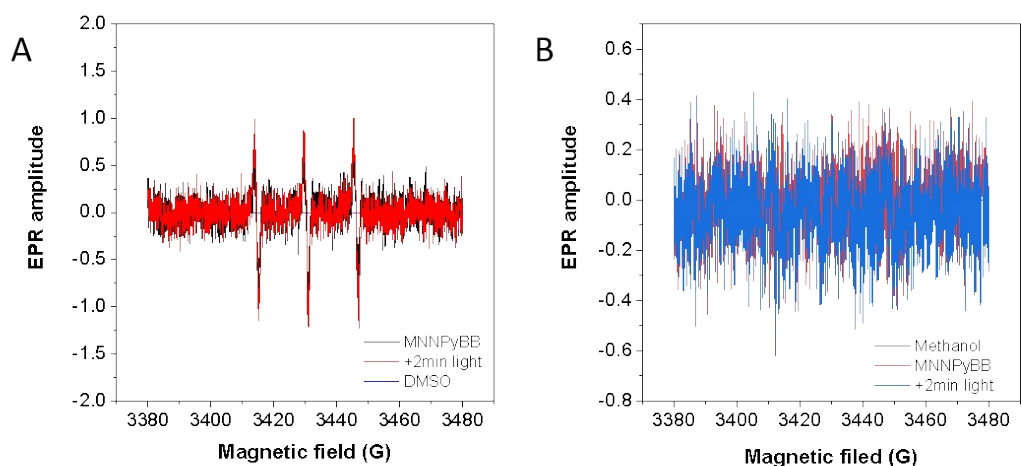


Figure S2 (A) The electron paramagnetic resonance (EPR) signal of TEMP for $^1\text{O}_2$ characterization in the presence of 1 mM MNNPyBB in DMSO. (B) The EPR signal of DMPO for $\cdot\text{OH}$ characterization in the presence of 1 mM MNNPyBB in methanol.

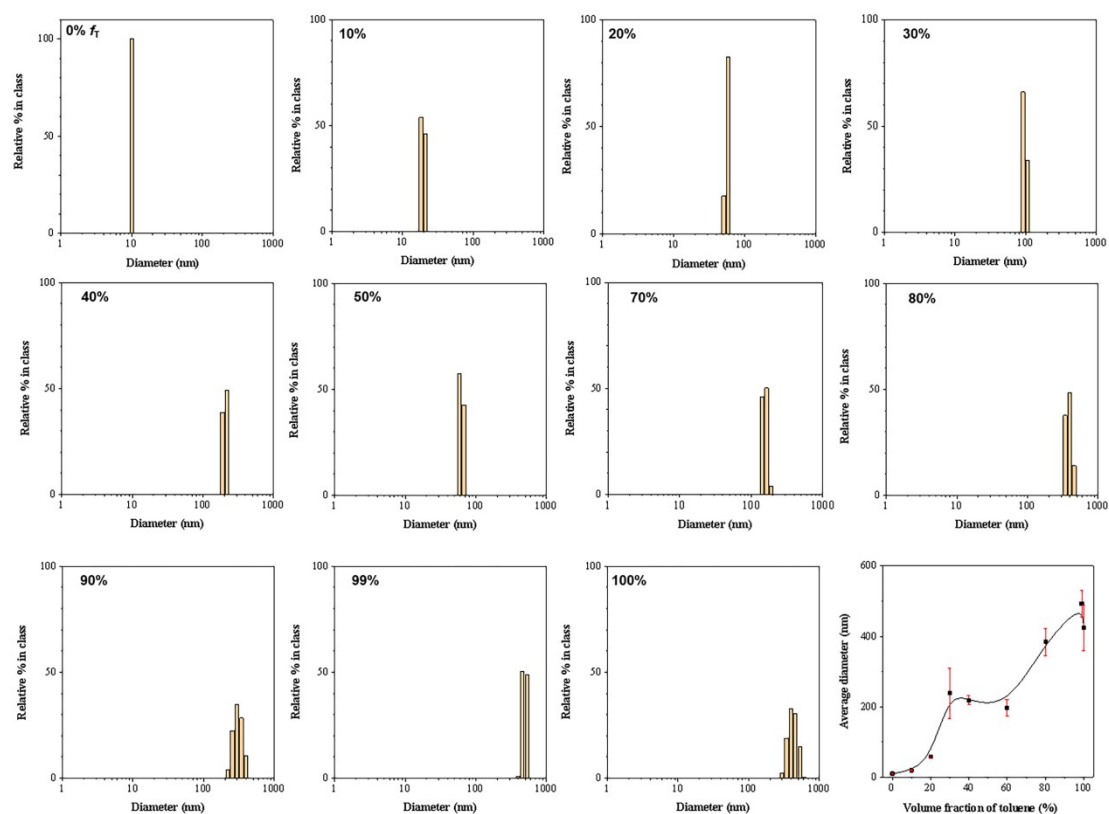


Figure S3 Size distribution of MNNPyBB in THF-toluene solutions with different volume fraction of toluene (f_T) and the average diameter plot along with the f_T .

S3 Bacterial toxicity of MNNPyBB with or without light

Table S1 the parameters of the bacterial strains

Strain name	Type
<i>E. coli</i>	ATCC 25922
<i>B. proteus</i>	ATCC 13315
<i>S. aureus</i>	ATCC 25923
<i>B. cereus</i>	ATCC 14579
<i>B. subtilis</i>	168, wb-800
MRSA	ATCC 43300

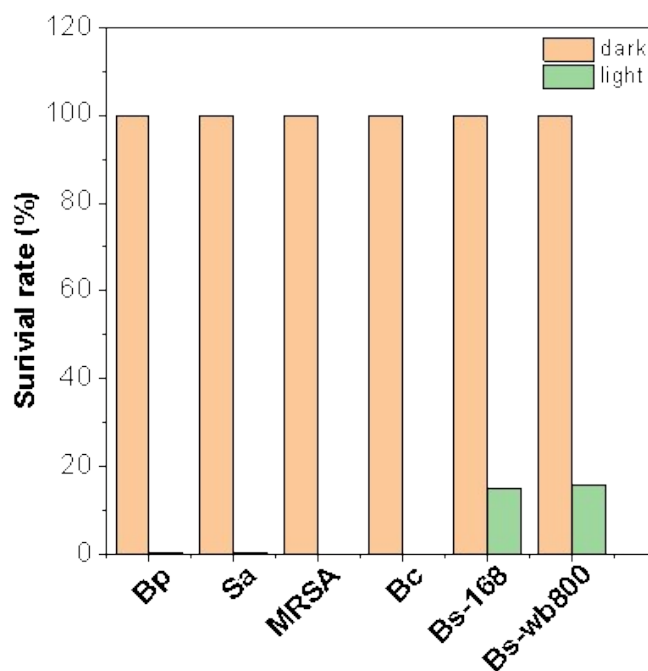


Figure S4 Relative colony count of bacteria upon MNNPyBB incubation with or without light exposure

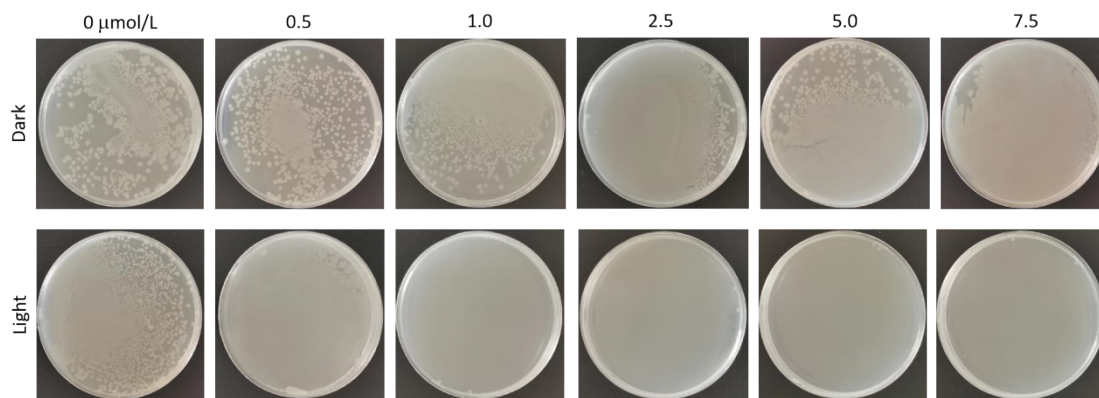


Figure S5 The spread plate results of antibacterial activity of MNNPyBB against *S. aureus* (ATCC 25923) with different concentration with or without light.

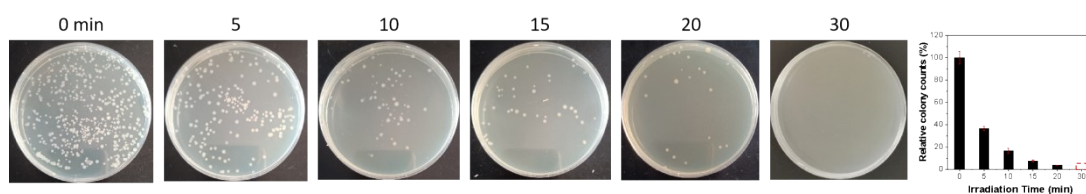


Figure S6 The spread plate results of antibacterial activity of MNNPyBB against *S. aureus* under light irradiation with different time.

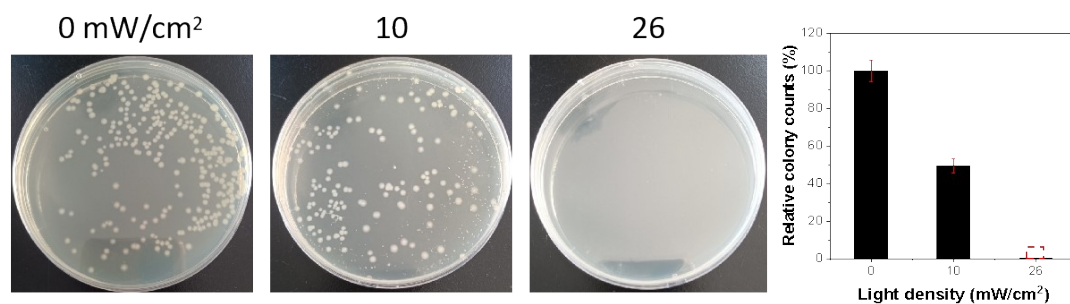


Figure S7 The spread plate results of antibacterial activity of MNNPyBB against *S. aureus* under light irradiation with different light energy density.

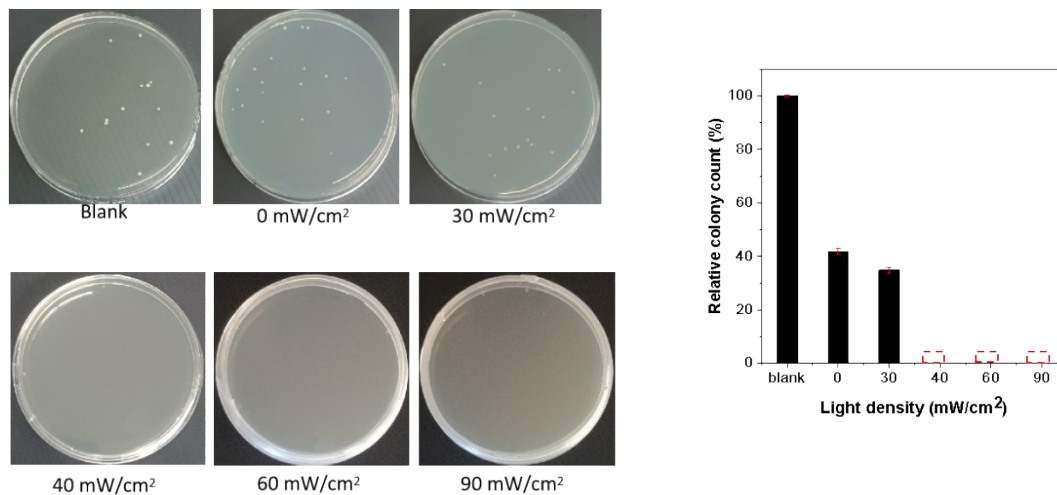


Figure S8 The spread plate results of antibacterial activity of MNNPyBB against MRSA under light irradiation with different light energy density. MRSA cells with different treatments were diluted 10^4 times before they were spread on the LB agar plates.

S4 Toxicity of MNNPyBB in Treated Mice

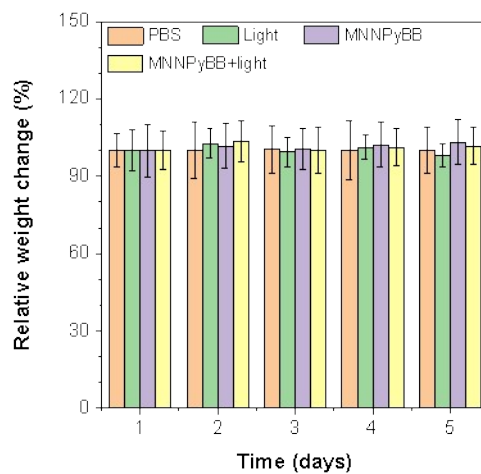


Figure S9 The relative weight of mice under different treatments

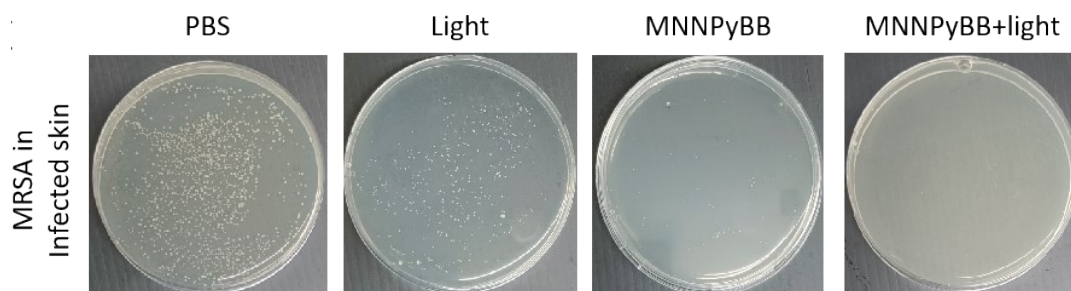


Figure S10 The spread plate results of MRSA cells in the infected skin of mice under different treatments.

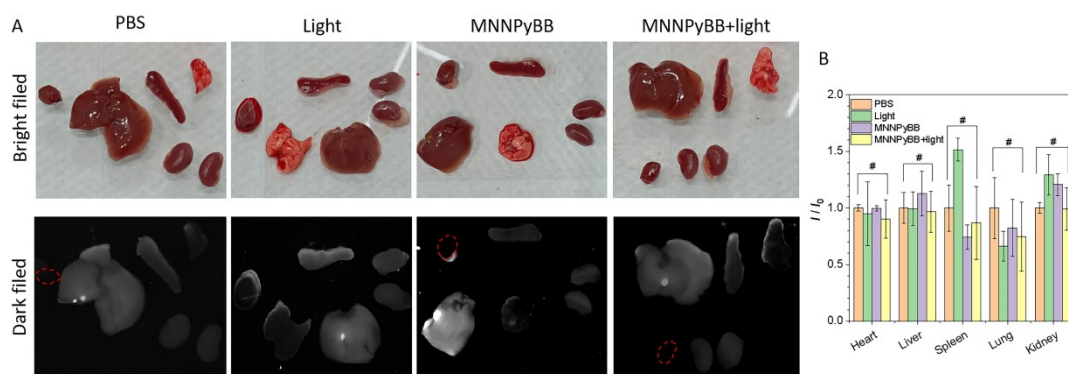


Figure S11 (A) The images, and (B) the relative MNNPyBB fluorescence signal of various important organs of mice under different treatments. The red circles in (A) referred to the location of the hearts.

For the fluorescence imaging experiments, mice from each group were randomly selected. Post-euthanasia, *in vitro* fluorescence imaging of the primary organs (heart, liver, spleen, lung, and kidney) was carried out using the Maestro EX fluorescence imaging system. The excitation light was chosen with a central wavelength of 505 nm, and fluorescence signals were collected in the spectral region of 700 nm.

In the practical applications of antibacterial agents, it is imperative for them to possess exceptional antibacterial efficacy while maintaining low toxicity and ensuring overall safety. In this study, MRSA was observed to accumulated exclusively at the inflammatory site without spreading to the bloodstream, let alone other tissues (Fig. 6A). So, the toxicity investigation of MNNPyBB was primarily focused on organs and tissues. *Ex vivo* fluorescence imaging of isolated organs (heart, liver, spleen, lung, and kidney) was conducted post-sacrifice of mice. Fortunately, no fluorescence signals were detected in the examined organs of mice treated with MNNPyBB and light (Fig. S12). However, mice treated solely with MNNPyBB exhibited a faint fluorescence signal in the liver. These results suggested that the locally injected MNNPyBB predominantly remained at the inflammatory site and did not migrate to other organs through the blood circulation in mice treated with MNNPyBB+L, implying a minimal risk of systemic side effects. A small fraction of MNNPyBB was metabolized by the liver and remained in the liver region of the group treated with MNNPyBB only. These findings confirmed that MNNPyBB+L treatment did not induce potential drug toxicity in mice, underscoring its excellent biosafety.

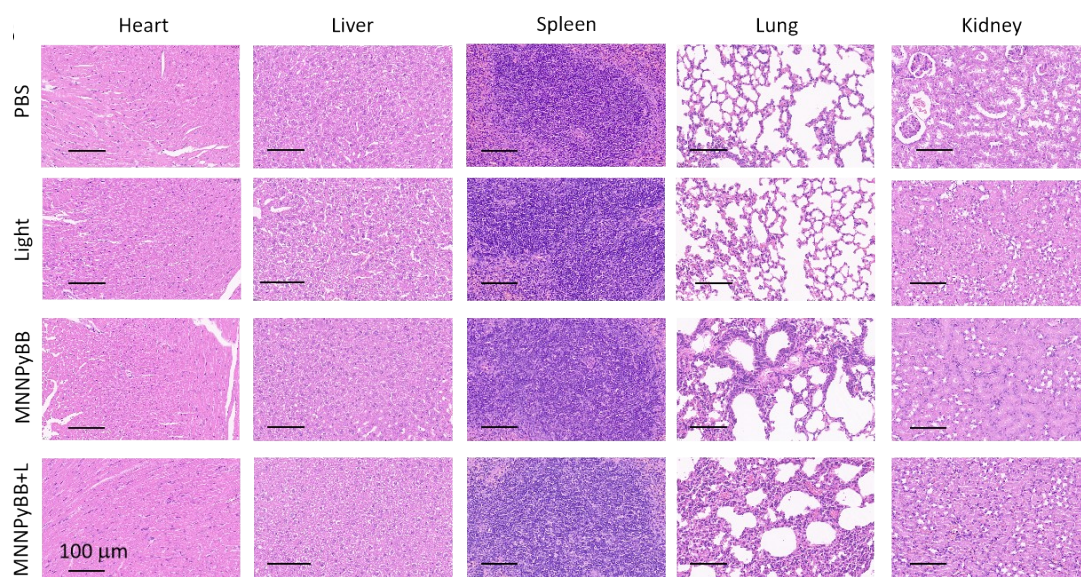


Figure S12 H&E staining of heart, liver, spleen, lung, kidney of mice treated with PBS, light alone, MNNPyBB alone and MNNPyBB+L.

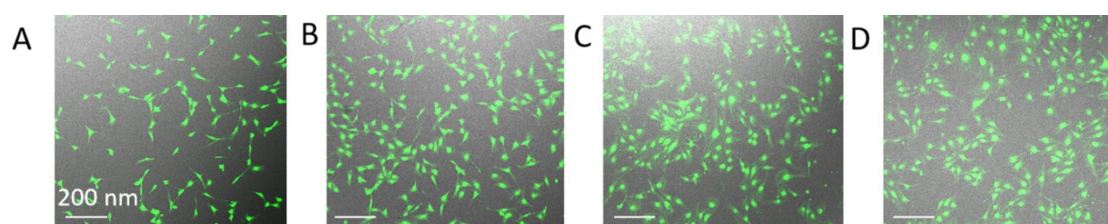


Figure S13 Fluorescence images of Calcein-AM incubated NIH3T3 and BEND.3 cells, (A) MNNPyBB incubated NIH3T3 cells in dark, (B) MNNPyBB incubated NIH3T3 cells under light, (C) MNNPyBB incubated BEND.3 cells in dark, (D) MNNPyBB incubated BEND.3 cells under light. 60 mW cm^{-2} , 10 min, λ_{Ex} : 490 nm, λ_{Em} : 515 nm, green fluorescent region for live cells and red for dead ones.

The biosafety of MNNPyBB, combined with its exceptional phototoxicity against bacteria, prompted an investigation of its potential toxicity towards mouse endothelial and epithelial cells [S11]. Embryonic fibroblasts NIH3T3 and mouse brain microvascular endothelial cells bEND.3 were chosen for this study [S12]. In both cell types incubated with MNNPyBB, no significant cell death was observed, regardless of whether light exposure was present or not (Fig. S13, 6B-C). When 3T3 cells were treated with MNNPyBB at a concentration of $5 \mu\text{mol L}^{-1}$, cell viability remained approximately 75.5%. Considering the practical cell density on the skin (1×10^{10} cells/cm²), which was 1.6×10^5 -fold higher than that of cultured bacterial cells (6.2×10^4 cells/cm²), the toxicity of MNNPyBB to skin cells was inferred to be negligible. Furthermore, the mild toxicity of MNNPyBB to 3T3 cells *in vitro* was deemed acceptable. Meanwhile, H&E staining indicated that MNNPyBB combined with white light did not induce damage or toxicity to the normal anatomical structure of various organs during the treatment period (Fig. S12). Collectively, these findings strongly

supported the potential of MNNPyBB+L as an effective and safe platform for treating chronic wound infections caused by MRSA bacteria.

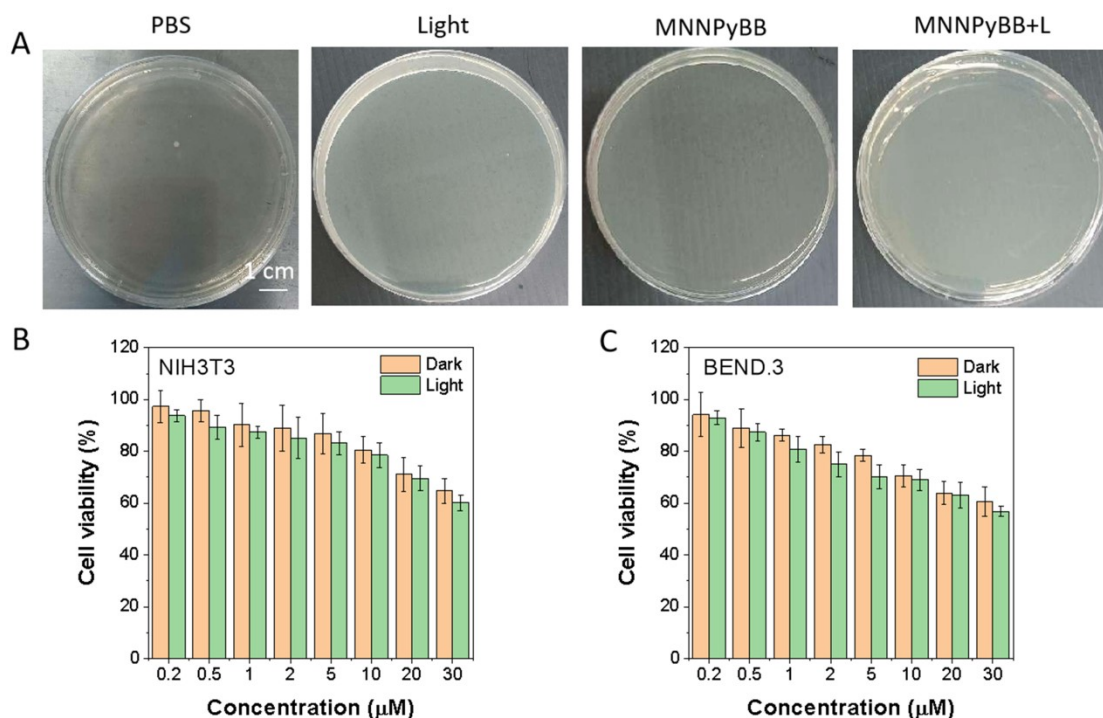


Figure S14 (A) Bacterial colony in the blood of PBS, light, MNNPyBB and MNNPyBB+L treated mice. (B-C) Cell viability of MNNPyBB incubated- (B) NIH3T3 and (C) BEND.3 cells with or without light irradiation, 60 mW cm^{-2} , 10 min.

S5 Optical properties and bacterial toxicity of intermediate MNNPy

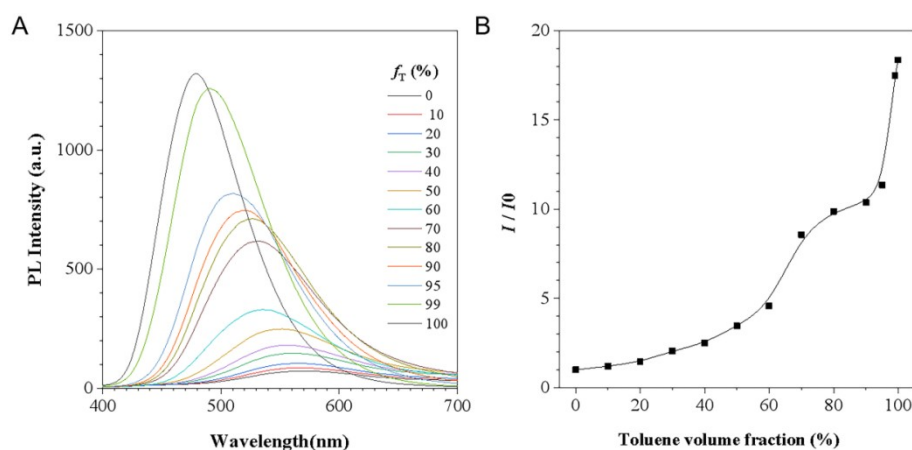


Figure S15 (A) The fluorescence spectra of MNNPy in THF-PhMe solutions with different PhMe volume fractions ($C_{\text{MNNPy}} = 10 \mu\text{M}$), (B) Plots of fluorescence intensity determined in THF-PhMe solutions *versus* PhMe fractions.

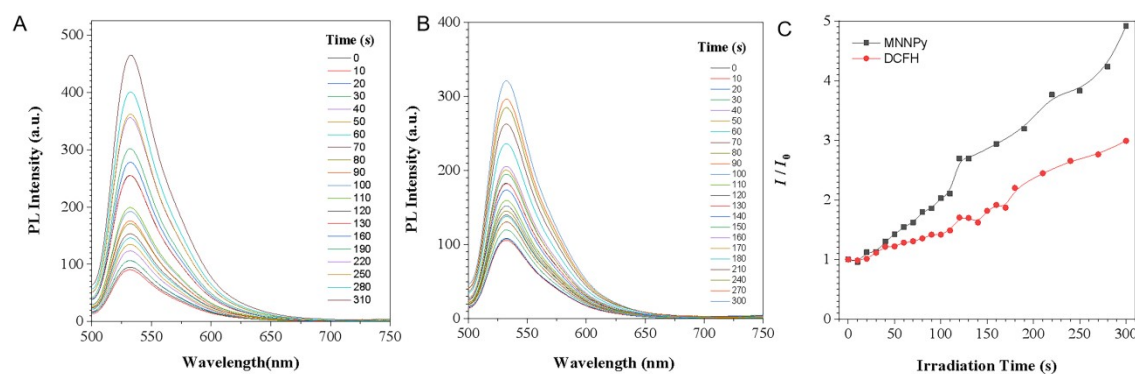


Figure S16 (A) Fluorescence emission of DCFH in the presence of MNNPy under light irradiation upon different time, (B) fluorescence emission of DCFH under light irradiation upon different time, (C) Polyline diagram of change in fluorescent intensity of dichlorofluorescein (DCF, 525 nm) with or without MNNPy.

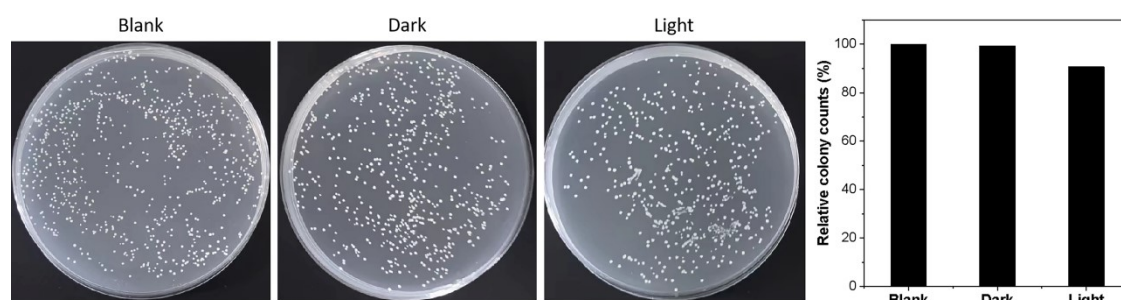


Figure S17 The spread plate results of antibacterial activity of MNNPy against MRSA with or without light and the relative colony counts results. $C_{MNNPy} = 50 \mu M$

Reference

- [S1] J. P. M. Jambeck, A. P. Lyubartsev, Derivation and systematic Validation of a Refined All-Atom Force Field for Phosphatidylcholine Lipids, *J. Phys. Chem. B* **2012**, *116*, 3164
- [S2] J. P. M. Jambeck, A. P. Lyubartsev, An extension and further validation of an all-atomistic force field for biological membranes, *J. Chem. Theory Comput.* **2012**, *8*, 2938
- [S3] J. P. M. Jambeck, A. P. Lyubartsev, Another piece of the membrane puzzle: Extending slipids further, *J. Chem. Theory Comput.* **2013**, *9*, 774
- [S4] I. Ermilova, A. P. Lyubartsev, Extension of the slipids force field to polyunsaturated lipids, *J. Phys. Chem. B*, **2016**, *120*, 12826
- [S5] F. Grote, A. P. Lyubartsev, Optimization of slipids force field parameters describing headgroups of phospholipids, *J. Phys. Chem. B*, **2020**, *124*, 8784
- [S6] J. Wang, R. M. Wolf, J. W. Caldwell, P. A. Kollman, D. A. Case, Development and testing of a general amber force field, *J. Comput. Chem.*, **2004**, *25*, 1157
- [S7] F. Neese, Software update: the ORCA program system, version 4.0, WIREs,

Comput. Mol. Sci., **2018**, *8*, e1327

[S8] F. Neese, Software update: The ORCA program system-Version 5.0, *WIREs Comput. Mol. Sci.* **2022**, *12*, e1606

[S9] T. Lu, F. Chen, Multiwfn: A Multifunctional Wavefunction Analyzer, *J. Comput. Chem.*, **2012**, *33*, 580

[S10] C. I. Bayly, P. Cieplak, W. D. Cornell, P. A. Kollman, A well-behaved electrostatic potential based method using charge restraints for deriving atomic charges: The RESP model, *J. Phys. Chem.*, **1993**, *97*, 10269

[S11] J. Kalucka, L. P. M. H. de Rooij, J. Goveia, K. Rohlenova, S. J. Dumans, E. Meta, N. V. Conchinha, F. Taverna, L.A. Teuwne, K. Veys, M. García-Caballero, S. Khan, V. Geldhof, L. Sokol, R. Chen, L. Treps, M. Borri, P. de Zeeuw, C. Dubois, T. K. Karakach, P. Carmelie, Single-cell transcriptome atlas of murine endothelial cells, *Cell*, **2020**, *180*, 4764

[S12] R. E Hynds, P. Bonfanti, S. M Janes, Regenerating human epithelia with cultured stem cells: feeder cells, organoids and beyond, *EMBO Mol. Med.*, **2018**, *10*, e8213